

Weakening temperature control on the interannual variations of spring carbon uptake across northern lands

Shilong Piao, Zhuo Liu, Tao Wang, Shushi Peng, Philippe Ciais, Mengtian Huang, Anders Ahlström, John Burkhart, Frederic Chevallier, Ivan A. Janssens, et al.

▶ **To cite this version:**

Shilong Piao, Zhuo Liu, Tao Wang, Shushi Peng, Philippe Ciais, et al.. Weakening temperature control on the interannual variations of spring carbon uptake across northern lands. Nature Climate Change, 2017, 7 (5), pp.359-363. ⟨10.1038/NCLIMATE3277⟩. ⟨hal-01584218⟩

HAL Id: hal-01584218

https://hal.science/hal-01584218v1

Submitted on 20 May 2019

HAL is a multi-disciplinary open access archive for the deposit and dissemination of scientific research documents, whether they are published or not. The documents may come from teaching and research institutions in France or abroad, or from public or private research centers.

L'archive ouverte pluridisciplinaire **HAL**, est destinée au dépôt et à la diffusion de documents scientifiques de niveau recherche, publiés ou non, émanant des établissements d'enseignement et de recherche français ou étrangers, des laboratoires publics ou privés.



HAL Authorization

Postprint of: Piao, S. "Weakening temperature control on the variations of spring carbon uptake across northern lands" in Nature climate change, vol. 7 (2017), p. 359-363. The final version is available at DOI 10.1038/nclimate3277

Weakening temperature control on the variations of spring carbon uptake across northern lands

Shilong Piao[1,2,3], Zhuo Liu[1], Tao Wang[2,3], Shushi Peng[1,4], Philippe Ciais[4], Mengtian Huang[1], Ivan A Janssens[5], Su-Jong Jeong[6], Xin Lin[4], Jiafu Mao[7], John Miller[8,9], Anwar Mohammat[10], Ranga B Myneni[11], Josep Peñuelas[12,13], Xiaoying Shi[7], Zhenzhong Zeng[1], Pieter P Tans[8]

[1] Sino-French Institute for Earth System Science, College of Urban and Environmental Sciences, Peking University, Beijing 100871, China

[2] Key Laboratory of Alpine Ecology and Biodiversity, Institute of Tibetan Plateau Research, Chinese Academy of Sciences, Beijing 100085, China

[3] Center for Excellence in Tibetan Earth Science, Chinese Academy of Sciences, Beijing 100085, China

[4] Laboratoire des Sciences du Climat et de l'Environnement, CEA CNRS UVSQ, Gif-sur-Yvette, France

[5] Department of Biology, University of Antwerp, Universiteitsplein 1, 2610 Wilrijk, Belgium

[6] Jet Propulsion Laboratory, California Institute of Technology, Pasadena, California 91011, USA

[7] Climate Change Science Institute and Environmental Sciences Division, Oak Ridge National Laboratory, Oak Ridge, TN, USA

[8] National Oceanic and Atmospheric Administration Earth Systems Research Laboratory (NOAA/ESRL), 325 Broadway, Boulder, CO 80305, USA

[9] Cooperative Institute for Research in Environmental Sciences, University of Colorado, Boulder, 80309 USA

[10] Xinjiang Institute of Ecology and Geography, Chinese Academy of Sciences, Urumqi 830011, Xinjiang, China

[11] Department of Earth and Environment, Boston University, 675 Commonwealth Avenue, Boston, MA 02215, USA

[12] CREAF, Cerdanyola del Valles, Barcelona 08193, Catalonia, Spain.

[13] CSIC, Global Ecology Unit CREAF-CEAB-CSIC-UAB, Cerdanyola del Valles, Barcelona 08193, Catalonia, Spain.

Manuscript for *Nature Geoscience*

Spring temperature controls the start of the carbon uptake (NEE) period and impacts the carbon balance of high latitude terrestrial ecosystems[1-3]. However, the mechanisms of temperature on NEE change over time. Here we use 34 years of atmospheric CO_2 concentration measurements at Barrow, Alaska (BRW, 71°N) to study the relationship between spring temperature and NEE. To do so, we use two indicators of CO_2 uptake in spring[1,2]: the spring zero crossing date (SZC, or day when the seasonal curve of CO_2 crosses down the detrended annual mean concentration) and the magnitude of the CO_2 drawdown from May to June (net spring carbon capture, SCC, or CO_2 difference between the first week of May and the last week of June). Our results show that the inter-annual correlation of SZC and SCC with spring land temperature (ST) was significant during the first 17 years but became non-significant during the last 17 years of the Barrow record. The sensitivity (linear regression slope) of both SZC and SCC to ST also decreased. Transport model simulations with the LMDZ model[4] coupled to net ecosystem carbon exchange (NEE) from ORCHIDEE land surface model[5] were used to separate the contributing factors. The simulation results suggest that the decline in the relationship of SZC and SCC with ST is mainly to NEE changes in boreal and arctic ecosystems (>50°N) rather than to wind changes. Furthermore, we show that the diminished response of Net Primary Productivity (NPP) to ST is the largest contributor to the weakening correlation of SZC and SCC with ST. This loss of northern NPP sensitivity to temperature variations is partly attributable to reduced chilling and increasing occurrence of extreme hot days in spring.

Boreal forests are estimated to have been a net sink of atmospheric CO_2 during the last decade[6], while Arctic tundra could be a sink or a small source[7]. Both modeling and observational studies show that spring warming advances leaf onset in the Northern Hemisphere, thus enhancing ecosystem photosynthetic activity and net carbon uptake as well[1-3,8]. A synthesis of flux measurements from 32 ecosystem sites[9] suggests that net CO_2 uptake in tundra during the growing season increased over the last 30 years. Warming induced enhanced CO_2 uptake by plants has been proposed as a mechanism to explain the earlier trend of the spring downward Zero-Crossing date (SZC, the day of the year when the seasonal CO_2 concentration crosses down the mean, Figure S1a). This was observed at Barrow (BRW, 71 ^{o}N) the longest Arctic atmospheric measurement station in northern of Alaska[1,10]. A strong negative correlation was shown between year-to-year SCZ variations at BRW and spring temperature across boreal and arctic regions[1,10]. Tree-ring data[11] and satellite vegetation greenness[12,13] further give hints that the response of northern terrestrial ecosystem carbon fluxes to temperature is not constant over time scales of decades.

Here, we investigate changes in the interannual relationship between spring temperature and northern CO_2 fluxes (NEE, net ecosystem exchange including disturbances). We use: (1) the long-term atmospheric CO_2 records from continuous air measurements at BRW; (2) the LMDZ4 atmospheric transport model[4] simulating CO_2 changes from NEE scenarios; (3) a set of process-based terrestrial carbon model simulations that provide these NEE scenarios and separate NEE into gross fluxes (Net Primary Production, NPP and heterotrophic respiration, HR); and (4) satellite observations of vegetation greenness, a proxy for photosynthetic potential. Temporal changes in the seasonal phase (and amplitude) of CO_2 at BRW reflect northern NEE

integrated by atmospheric mixing[1,14], with a footprint dominated by high latitude ecosystems in Alaska, boreal North America and Europe, and eastern Siberia[15]. Like previous studies[1,2,16], the temporal correlations of both SZC (Figure S1, Figure S2a) and SCC (the seasonal drop of CO_2 between the first week of May and the last week of June, Figure S1, Figure S2b) with temperature are used to quantify the temperature response of spring NEE. The average spring temperature from March to June (ST) was used as predictor of SZC and SCC, since these months show the strongest negative ST correlation with SZC and positive correlation with SCC (Figure S3) (all variables being detrended, see Methods).

The significant negative Pearson partial correlation between SZC and ST (R_{szc}) over vegetated lands (north of 50^o N) found in the above-cited studies is confirmed when from the full BRW record spanning from 1979 to 2012. Partial correlation allows to remove the effect of other variables that co-vary with ST in affecting NEE, such as precipitation and radiation (here approximated by cloudiness). The main result is that the partial correlation between SZC and ST (R_{szc}) which was of -0.84 during the first period (1979-1995) decreased down to -0.11 during the second period (1996-2012) (Figure S4a). Further partial correlation analyses randomly selecting 14 years of the first period (the number of degrees of freedom being 10) show that all the 680 selections have significant negative correlation between SZC and ST at the significance level of 0.05 (Figure 1a). In contrast, only 15 (2%) selections conserved a (marginally) significant negative correlation between SZC and ST during the second period (R_{szc} variable from -0.77 to 0.47, Figure 1a). Multiple linear regression analysis using SZC as dependent variable and the spatial average of temperature, precipitation, and cloudiness as independent variables further indicate that the interannual sensitivity (linear regression

coefficient) of SZC to ST (γ_{szc} ; Figure S3a) significantly decreased from -4.33 ± 1.70 days $^{o}C^{-1}$ during the first period down to -0.82 ± 4.32 days $^{o}C^{-1}$ during the second period ($P<0.05$) (see Figure S5a). This decrease in γ_{szc} should be viewed however with caution because of correlations between SZC and ST becoming non-significant during the second period.

The same analysis using SCC instead of SZC yields similar results (Figure 1b). For example, the partial correlation between SCC and ST (R_{scc}) decreased from 0.70 ($P<0.05$) in the first period to 0.19 in the second period ($P=0.50$) during 1996-2012. The interannual sensitivity of SCC to ST (γ_{scc}) also significantly decreased ($P<0.05$) from 1.08 ± 0.65 ppm $^{o}C^{-1}$ to 0.31 ± 0.96 ppm $^{o}C^{-1}$ (Figure S5b).

To further test the robustness of the decline of R_{szc} and R_{scc}, we applied the same partial correlation analysis using different climate data sets (Figure S6), defining preseason (the period before June for which the correlation between SZC or SCC and temperature was the highest, see Methods) (Figure S7), using weekly CO_2 data from BRW instead of daily data (Figure S8), and statistically controlling for co-variation in snow water equivalent[17] or winter temperature in addition to precipitation and cloudiness (Figure S9). All these tests confirm a decrease of R_{szc} and R_{scc}. In addition to the BRW record, a significantly decline of R_{szc} and R_{scc} is also observed with the CO_2 records of Cold Bay (CBA) and Station M (STM), two long term high latitude stations (Figure S10). Compared to BRW, however, STM located in the North Atlantic shows an average weaker correlation between SZC, SCC and ST during the first period (Figure S10). Finally, the gradual decrease of R_{szc} and R_{scc} (Fig. S4) with time further indicates that the observations in Fig. 1 are robust to the choice of two periods (e.g., 1996 in Fig. 1).

We tested the following hypotheses to explain the decrease of R_{szc} and γ_{szc}: (H1a), there is a decreasing sensitivity of NEE to ST because net primary productivity (NPP) is becoming less sensitive to temperature while the sensitivity of Heterotrophic Respiration (HR) is stable; (H1b) HR is becoming less sensitive to temperature anomalies and the sensitivity of NPP is stable over time; (H2) the SCZ changes is not due to ecosystem fluxes but to changes in atmospheric transport.

To test these hypotheses, we performed a set of factorial simulations with a model of NEE (ORCHIDEE) coupled to an atmospheric transport model (LMDZ4) with the option of variable winds over the last 34 years (Table S1). Daily NEE from ORCHIDEE forced by climate fields[18] and rising atmospheric CO_2 [5] was prescribed to LMDZ4 to simulate CO2 at BRW during 1979-2012 (see Methods). Note that the version of ORCHIDEE used here does not include disturbance (fire) emissions but NPP and HR driven by variable climate and CO_2. The list of factorial simulations summarized in Table S1 includes three simulations with variable transport, one with climatological NEE (FIX-NEE), interannual NEE (VAR-NEE), and interannual NEE only over boreal regions (VAR-NEE-BOR). The contribution of interannual NEE to the variability in SZC and SCC is estimated by the difference between TFTT and CFTT (refer to as the TFCT simulation), while the difference between TFTT-B and CFTT (refer to as the TFCT-B simulation) is used to separate the contribution of boreal NEE variability of SZC and SCC (see Methods). Consistent with ref. (15) interannual variation in both SZC and SCC are found to be primarily explained by variation in NEE in regions north of 50°N (Figure S11).

The observed weakening of R_{szc} (Figure 1a and S4a) is captured by both simulations TFCT and TFCT-B, indicating that changes in the correlation between SZC and ST primarily reflect

the temperature response of NEE. Consistent with observations, TFCT-B also shows a decreased correlation, with R_{szc} being of 0.73 during the first period and becoming non-significant during the second period (-0.33). In contrast, SZC derived from the CFTT simulation with variable atmospheric transport, shows no significant correlation with ST (Figure 1a and S4a). Similar results are obtained for SCC (Figure 1b and Figure S4b). These model results are consistent with both hypothesis H1a and H1b, and suggest that changes in interannual NEE rather than in transport explains the loss of correlation between ST and SZC over time.

The BRW records of SZC over the last three decades reflect different processes: interannual climate affecting NEE predominantly via (1) NPP, (2) HR, (3) natural disturbances (fire, or wind-throw), and slow changes in vegetation structure and function indirectly affecting the interannual response of NPP, HR and disturbances. Two different types of slow changes in northern vegetation could modulate the interannual response of NEE and explain the observed loss of correlation between SZC and ST: (1) changes in non-managed vegetation (e.g. shrubification in the Arctic), and (2) trends of fluxes from managed ecosystems, including human-induced disturbances of NPP such as harvest of crops and forests and land-use change[19,20]. In addition, changes in air-sea CO_2 fluxes and in the seasonality and spatial distribution of fossil fuel emissions transported to BRW might also influence SZC but the relationship between these fluxes and ST is less documented.

Compared to these plausible real-world processes, the results of TFCT-B simulation only include the effects of climate change and rising atmospheric CO_2 (fertilization effect) on NPP and HR. We therefore performed two additional simulations: (1) TFCT-T where only temperature is varied, other driving variables being held constant, and (2) TFCT-TP where both

temperature and precipitation are varied (see Methods, and Supplementary Table S1). As shown in Figure 1a and Figure S5a, TFCT-T reproduces a decrease of R_{szc} and γ_{szc} (the difference between the first and second period). Furthermore, temporal variations in R_{szc} from TFCT-T are very similar to those from TFCT-B where all climate drivers are varied (Figure S4a). This implies that in the ORCHIDEE-LMDZ4 model, the decrease of R_{szc} and γ_{szc} is mainly attributed to changes in the temperature response of NEE in boreal regions rather than to other climate factors. Replacing SZC with SCC produced similar results (Figure 1b and Figure S5b).

For testing H1a against H1b, we performed two additional simulations using NEE derived (1) from daily variable HR for 1979 and interannually varying NPP (TFCT-NPP), and (2) from daily variable NPP for 1979 and interannually varying HR (TFCT-HR) (see Method and Table S1). As shown in Figure 1, a significant decrease of R_{szc} and R_{scc} was produced by TFCT-NPP, but not by TFCT-HR (see also Figure S4). This suggests that changes in the interannual temperature response of NPP rather than HR explain most of the decrease of R_{szc} and R_{scc}.

We propose two possible mechanisms for the correlation between ST and NPP becoming weaker. The first mechanism is based on the fact that spring NPP (and leaf) onset is partly controled by chilling during the dormancy period in winter, and that winter warming may result in loss of chilling so that warmer springs will not advance NPP any more [21]. We indeed found a significant declining trend in NCD over the last 3 decades (Figure S12 and Figure S13a). To test the importance of this mechanism, we performed an additional simulation TFTT-D where only temperature out of the dormancy period (November-April) is varied to simulate NEE in ORCHIDEE (see methods and Table S1). The difference between simulation TFTT-T and TFTT-D is denoted as TFCT-D, indicating the impacts of NCD on land carbon flux. As shown

in Figure 1a, TFCT-D explains a decrease of R_{SZC} from -0.73 during the first 17 years to -0.50 during the last 17 years. In addition, we plotted the spatial distribution of changes in partial correlation coefficient (R_{NEE-T}) between ST and simulated NEE north of 50° N during the last 3 decades. The results show that eastern Siberia, parts of Alaska, and northern Europe are the regions where a significant decrease in R_{NEE-T} happened (Figure 2a) resulting mainly from a decrease in the correlation between ST and NPP (R_{NPP-T}) (Figure 2b). This pattern is roughly similar with that from the difference between S4 and S1 (Figure 2g, h), suggesting that the loss of chilling contributed to the weakened R_{NEE-T} (mainly R_{NPP-T}).

The second, mechanism to account for the decreased correlation between ST and NPP is that a change in the number of extreme hot days (NHD) occurred during March-June over the last 3 decades, and reduced NPP in spring[22]. We observed an increase in NHD during March-June during the last 30 years, particularly in northern and eastern Siberia (Figure S13b), which could explain both satellite-observed and ORCHIDEE-simulated decreasing trends of correlation between vegetation productivity and ST in these regions (Figure 2a-f, j).

The decrease in R_{NEE-T} is often larger in regions that experienced a large decrease in NCD (the bottom left of Figure 3a) or a large increase in NHD (the top right of Figure 3a). This pattern was much more similar to that of change in R_{NPP-T} (Figure 3b) than that in R_{HR-T} (Figure 3c) and pattern of change in R_{NPP-T} were similar to those deduced from NDVI data (Figure 3d). We detected an unexpected increase in R_{NEE-T} in a region * describe where it is %* central asia that has experienced both a large decrease in NCD and a large increase in NHD (Figure 3a). This region outlined in black (mainly 70°E-95°E，50°N -58°N) has experienced a large increase in spring precipitation over the last 3 decades (Figure S13c). Given that cropland mainly

occupies this region and there is a high sensitivity of cropland productivity to water conditions[24, 25], the negative impacts of decreased NCD and increased NHD on spring C uptake may be reversed by increasing precipitation in this region. Besides mechanisms related to NCD and NHD changes, the response of vegetation productivity (and of phenology controlling productivity) to temperature is nonlinear[26], and may decrease in response to global warming[13]. In addition, changes in disturbance regimes associated with fire[27] may also have played a role.

Our analysis based on interannual variability should be distinguished from the previous long-term trend analysis[14] documenting a continuous increase in seasonal CO_2 exchange over the last 3 decades. Recent studies have demonstrated that besides climatic change, the long-term trends in seasonal CO_2 exchange are mainly driven by increasing CO_2 concentrations[28, 29], increasing nitrogen deposition[30] and agricultural intensification[19, 20]. The result presented in this study suggests that the 'warmer spring / bigger sink' mechanism may not be persistent over several decades. It clearly demonstrates the need for long-term in situ measurements and their value in giving us understanding of the dynamics of the response of the terrestrial carbon balance to climate change. Our results are also relevant to predicting feedbacks between the terrestrial carbon cycle and global climate system. If the decline in the positive impact of temperature on boreal carbon uptake continues, the ability of the northern ecosystem to sequester carbon may be reduced or even reversed in the future.

Methods

Atmospheric CO_2 concentration data. Daily atmospheric CO_2 concentration records

constructed from surface in-situ continuous measurements at Point Barrow (BRW), Alaska, were obtained from the National Oceanic and Atmospheric Administration (NOAA) Earth System Research Laboratory archive[31] for the period of 1979-2012. In order to separate the seasonal cycle from the long-term increase in CO_2, the daily data was firstly fitted with a function consisting of a quadratic polynomial for the long-term trend and four-harmonics for the annual cycle[32]. The residuals from this function fit are then obtained. A smooth curve is obtained by digitally removing the short term variation from the residuals using 1.5 month (or 1.0 month, see Figure S7) Full-Width Half-Maximum value (FWHM) averaging filter and then adding the filtered residuals to the fitted function. A deseasonalized long-term trend is obtained by digitally filtering the residuals using 390-days FWHM averaging filter and then adding the filtered residuals to the quadratic polynomial long-term trend. The difference between the smooth curve and the deseasonalized long-term trend is then used to represent the detrended seasonal CO_2 curve. Note that any data lying outside 5 (or 3, 2.5, see Figure S7) standard deviations of the residuals between the original data and the smooth curve are regarded as outliers and discarded from the original daily time series[33]. This procedure was repeated until no outliers were identified. The spring (downward) zero-crossing date (SZC) for each year was then determined as the day when the sign of the seasonal CO_2 excursion from the annual mean trend changed from positive to negative (Figure S1). Based on the detrended seasonal CO_2 curve, the mean estimate of SZC over the period of 1979-2012 at BRW site is around day of the year (DOY) 180 with an interannual variability of 3.5 days (DOY range from 173 to 188). The seasonal maximum of atmospheric CO_2 occurs systematically during the period from late April to early May. Defining spring as the months of May-June, the change in CO_2 over this

spring period (hereafter SCC) was also computed for each year from the detrended seasonal CO_2 cycle (Figure S1). We also used weekly atmospheric CO_2 concentration records, based on either surface in-situ continuous measurements or surface flask samples, from the Earth System Research Laboratory of the National Oceanic and Atmospheric Administration (NOAA)[34] at BRW site (Figure S8) and derived similar results. Furthermore, weekly atmospheric CO_2 concentration records based on surface flask samples at the Point Cold Bay (CBA) and Ocean Station M (STM) site[34] that have relatively longer observations (34 years and 29 years, respectively) were also used in this study (Figure S10). We do not perform outlier detection for weekly data since CO_2 concentration records have been processed (smoothed, interpolated, and extrapolated) in GLOBVIEW-CO_2 product to address issues of temporal discontinuity and data sparseness in atmospheric observations.

Climate data. Monthly climate data (temperature, precipitation and cloud cover) at a spatial resolution of 0.5° from 1901 to 2012 were taken from the University of East Anglia's Climate Research Unit CRU TS 3.2 data set[35]. We also applied another two climate data sets (Climatic Research Unit-National Centers for Environmental Prediction (http://dods.extra.cea.fr/data/p529viov/cruncep/) and Watch Forcing Data methodology applied to ERA-Interim data (http://www.eu-watch.org/gfx_content/documents/README-WFDEI.pdf)), and returned very similar results (Figure S6). Snow water equivalent was derived from the European Space Agency (ESA)'s Global Snow Monitoring for Climate Research (GlobSnow) product that is generated by combining satellite data with ground measurements of snow depth[17].

Satellite Normalized Difference Vegetation Index (NDVI) data. We used the third Normalized Difference Vegetation Index (NDVI3g) data product generated from Advanced

Very High Resolution Radiometer (AVHRR) data by the Global Inventory Monitoring and Modeling Studies (GIMMS)[36]. AVHRR NDVI3g has a spatial resolution of 8 km and a repeat cycle of 15 days for 1982-2011. This product has been carefully assembled from different AVHRR sensors, removing several detrimental effects, such as calibration loss, orbit drift, volcanic eruption.

Terrestrial carbon-cycle model. ORCHIDEE (Organizing Carbon and Hydrology In Dynamic Ecosystems) is a process-based model that calculates the fluxes of CO_2, H_2O and heat between the atmosphere and the land surface on a half-hourly basis and the variations in the water and carbon pools on a daily basis[5]. In this study, we used the version that was used in the IPCC AR5. ORCHIDEE simulates carbon cycle processes such as half-hourly photosynthesis, as well as carbon allocation, litter decomposition, soil carbon dynamics, maintenance and growth respiration, and phenology at the daily time step. ORCHIDEE has been widely used for investigating terrestrial carbon-cycle dynamics and their responses to climate variations.

We ran the ORCHIDEE model until the carbon pools reached equilibrium after about 1000 years. We used a resolution of 0.5 degree, with 1901 climate data and the 1860 atmospheric CO_2 concentration of 286.05 ppm. The model was then run to 1978 with a transient climate and corresponding observed atmospheric CO_2 concentration during that period. Note that because there are no climate data during 1860-1900, the transient 1901-1910 climate was recycled for 1860-1900. For years 1979-2012, we performed three different simulations (S1, S2, S3 and S4). In simulation S1, only temperature was varied. In simulation S2, only temperature and precipitation were varied. In simulation S3, atmospheric CO_2 and all climatic factors were varied. In simulation S4, only temperature out of the dormancy period was varied. The

difference between simulation S1 and S4 indicates the effects of the number of chilling days during the dormancy period on the correlation between spring C flux and temperature.

Atmospheric transport model. We used LMDZ4, a 3D atmospheric tracer transport model from the Laboratoire de Météorologie Dynamique[4], nudged with horizontal winds from the ECMWF reanalysis, to transform NEE from ORCHIDEE into a point estimate of CO_2 concentration at BRW station. To separate the effects of transport and terrestrial carbon fluxes on the SZC and SCC signal, we performed three transport simulations with interannual varying winds (see Table S1). The first one gave us the interannual daily NEE fluxes calculated during the period 1979–2012 by simulation S3 (TFTT). The second simulation (referred to as CFTT simulation, see main text) used climatological but daily variable NEP for 1979 derived from simulation S3. The third simulation is similar with TFTT, but use interannual daily NEE fluxes for only north of 50 ^{o}N (TFTT-B). The contribution of interannually varying fluxes to the variability in SZC and SCC is assessed by the difference in simulated atmospheric CO_2 between the first and the second simulations, which we refer to as the TFCT simulation. The difference between TFTT-B and CFTT is used as contribution of boreal and arctic fluxes to the variability in SZC and SCC (refer to as TFCT-B). Two daily NEE outputs from ORCHIDEE (S1 and S2) over the period 1979-2012 were fed into the transport model to derive their respective daily CO_2 concentrations at BRW station. To further separate the relative roles of NPP and HR, we also performed two additional transport simulations using daily NEE calculated (1) from interannually varying NPP and climatological HR based on the S3 simulation, and (2) from interannually HR and climatological NPP based on the S3 simulation. Using similar method of estimation as used in the TFCT-B simulation, we calculated the contribution of temperature

change (referred to as TFCT-T simulation), both temperature and precipitation change (referred to as TFCT-TP simulation), interannually varying NPP fluxes (referred to as TFCT-NPP simulation), and interannually varying HR fluxes (referred to as TFCT-HR simulation) over north of 50 ^{o}N (see Table S1).

Analysis Spring vegetation activity is highly associated with the temperatures in the preceding months. We determined the length of the preseason whose average temperature had the largest influence on SZC and SCC by calculating the correlation coefficients of SZC and SCC with temperature during the 0, 1, 2, 3 … 7 months before June (SZC over the period of 1979-2012 at BRW site is around day of the year (DOY) 180). We found that the average temperature from March to June (ST) was most strongly negatively correlated with SZC (highest positive correlation with SCC) at BRW for 1979-2012 and thus used the average temperature during these months. Then we calculated correlation coefficient of SZC and SCC with ST for the earliest 17 years (1979-1995) and the more recent 17 years (1996-2012), through randomly selecting 14 years among the corresponding period. A two-sample t-test was conducted to determine whether there is a statistically significant difference of Rszc (or Rscc) between the first (1979-1995) and second (1996-2012) half study period. Note that the variability of ST is comparable during the two periods and should not be a factor in the breakdown. Using a similar method, for each randomly selected period (e.g., 14 of 17 years during the first half study period (1979-1995)), we also defined preseason (the period before June for which the negative correlation between SZC and temperature (positive correlation for SCC) was highest) to further assess the robustness of the inferred decline of Rszc and Rscc over the last three decades (Figure S7).

We performed partial correlation analyses between SZC (SCC) and ST (R_{szc} and R_{scc}) after statistically controlling for interannual variation in precipitation and cloud cover during the period from March to June. The partial correlation coefficient R_{SZC} (R_{SCC}) is computed as the correlation between the residuals calculated after regressing SZC (SCC) on precipitation and cloud cover and those after regressing ST on precipitation and cloud cover. The interannual sensitivity of SZC (γ_{szc}) to ST variation was computed as the partial regression coefficient of ST in a multiple linear regression of SZC against temperature, precipitation and cloud cover during the period from March to June. We apply the same approach to calculate interannual sensitivity of SCC (γ_{scc}) to ST variation. Temperature, precipitation and cloud cover were computed as the spatial average weighted by NDVI over the vegetated land area to the north of 50°. The vegetated land area is defined as grid points where the average of annual mean NDVI over the period of 1982–2011 is larger than 0.1. All variables were linearly detrended over the study period before the regression analyses were performed.

References

1. Keeling, C. D., Chin, J. F. S. & Whorf, T. P. Increased activity of northern vegetation inferred from atmospheric CO_2 measurements. *Nature* **382,** 146–149 (1996).
2. Randerson, J. T., Field, C. B., Fung, I. Y. & Tans, P. P. Increases in early season ecosystem uptake explain recent changes in the seasonal cycle of atmospheric CO_2 at high northern latitudes. *Geophys. Res. Lett.* **26,** 2765–2768 (1999).
3. Richardson, A. D. *et al.* Influence of spring and autumn phonological transitions on forest ecosystem productivity. *Phil. Trans. R. Soc. B* **365,** 3227-3246 (2010).
4. Hourdin, F. *et al.* The LMDZ4 general circulation model: Climate performance and

sensitivity to parametrized physics with emphasis on tropical convection. *Clim. Dyn.* **27,** 787–813 (2006).

5. Krinner, G. *et al.* A dynamic global vegetation model for studies of the coupled atmosphere–biosphere system. *Glob. Biogeochem. Cycles* **19,** doi:10.1029/2003GB002199 (2005).
6. Dolman, A. J. *et al.* An estimate of the terrestrial carbon budget of Russia using inventory-based, eddy covariance and inversion methods. *Biogeosciences* **9,** 5323–5340 (2012).
7. McGuire, A. D. *et al.* An assessment of the carbon balance of Arctic tundra: comparisons among observations, process models, and atmospheric inversions. *Biogeosciences* **9,** 3185–3204 (2012).
8. Black, T. A. et al. Increased carbon sequestration by a boreal deciduous forest in years with a warm spring. *Geophys. Res. Lett.* **27,** 1271–1274 (2000).
9. Belshe, E. F., Schuur, E. A. G. & Bolker, B. M. Tundra ecosystems observed to be CO_2 sources due to differential amplification of the carbon cycle. *Ecol. Lett.* **16**, 1307-1315 (2013).
10. Barichivich, J. *et al.* Large-scale variations in the vegetation growing season and annual cycle of atmospheric CO_2 at high northern latitudes from 1950 to 2011. *Glob. Change Biol.* **19,** 3167-3183 (2013).
11. D'Arrigo, R. D. *et al.* Thresholds for warming-induced growth decline at elevational tree line in the Yukon Territory, Canada. *Glob. Biogeochem. Cycles* **18,** GB3021 (2004).
12. Angert, A. *et al.* Drier summers cancel out the CO_2 uptake enhancement induced by warmer springs. *Proc. Natl Acad. Sci. USA* **102,** 10823–10827 (2005).

13. Piao, S. L. *et al*. Evidence for a weaking relationship between interannual temperature variability and northern vegetataion activity. *Nat. Commun.* **5,** doi:10.1038/ncomms6018 (2014).

14. Graven, H. D. *et al*. Enhanced seasonal exchange of CO_2 by northern ecosystems since 1960. *Science* **341,** 1085-1089 (2013).

15. Kaminski, T., Giering, R. & Heimann, M. Sensitivity of the seasonal cycle of CO_2 at remote monitoring stations with respect to seasonal surface exchange fluxes determined with the adjoint of an atmospheric transport model. *Phys. Chem. Earth* **21,** 457-462 (1996).

16. Piao, S. L. *et al.* Net carbon dioxide losses of northern ecosystems in response to autumn warming. *Nature* **451,** 49-52 (2008).

17. Takala, M. *et al.* Estimating Northern Hemisphere snow water equivalent for climate research through assimilation of space-borne radiometer and ground-based measurements. *Remote Sens. Environ.* **115,** 3517–3529 (2011).

18. Viovy, N. & Ciais, P. *CRUNCEP data set for 1901–2012, Version 4* <http://dods.extra.cea.fr/data/p529viov/cruncep> (2014).

19. Gray, J. M. *et al.* Direct human influence on atmospheric CO_2 seasonality from increased cropland productivity. *Nature* **515,** 398–401 (2014).

20. Zeng, N. *et al.* Agricultural Green Revolution as a driver of increasing atmospheric CO_2 seasonal amplitude. *Nature* **515,** 394–397 (2014).

21. Fu, Y. S. *et al.* Declining global warming effects on the phenology of spring leaf unfolding. *Nature,* **526,** 104-107 (2015).

22. Wahid, A., Gelani, S., Ashraf, M. & Foolad, M. R. Heat tolerance in plants: an overview.

Environ. Exp. Bot. **61**, 199-223 (2007).

23. Atkin, O. K. & Tjoelker, M. G. Thermal acclimation and the dynamic response of plant respiration to temperature. *Trends Plant Sci.* **8**, 343-351 (2003).
24. Connor, D. J., Loomis, R. S. & Cassman, K. G. *Crop ecology: productivity and management in agricultural systems* (Cambridge Univ. Press, 2011).
25. Lobell, D. B. *et al*. Greater sensitivity to drought accompanies maize yield increase in the US Midwest. *Science* **344**, 516-519 (2014).
26. Yamori, W., Hikosaka, K. & Way, D. A. Temperature response of photosynthesis in C3, C4, and CAM plants: temperature acclimation and temperature adaptation. *Photosynth. Res.* **119,** 101–117 (2014).
27. Kasischke, E. S. *et al.* Alaks's changing fire regime-implications for the vulnerability of its boreal forests. *Can. J. For. Res.* **40,** 1313–1324 (2010).
28. Schimel, D., Stephens, B. B. & Fisher, J. B. Effect of increasing CO_2 on the terrestrial carbon cycle. *Proc. Natl Acad. Sci. USA* **112**, 436-441 (2015).
29. Forkel, M. *et al*. Enhanced seasonal CO_2 exchange caused by amplified plant productivity in northern ecosystems. *Science* 10.1126/science.aac4971 (2016).
30. Galloway, J. N. *et al*. Nitrogen cycles: past, present, and future. *Biogeochemistry* **70**, 153-226 (2004).
31. Thoning, K. W., Kitzis, D. R. & Crotwell, A. *Atmospheric Carbon Dioxide Dry Air Mole Fractions from quasi-continuous measurements at Barrow, Alaska*. <http://dx.doi.org/10.7289/V5RR1W6B> (NOAA ESRL Global Monitoring Division, Boulder, CO, 2014).

32. Thoning, K. W., Tans, P. P. & Komhyr, W. D. Atmospheric carbon dioxide at Mauna Loa observatory. 2. Analysis of the NOAA GMCC data, 1974-1985. *J. Geophys. Res.* **94,** 8549–8565 (1989).

33. Harris, J. M. *et al.* An interpretation of trace gas correlations during Barrow, Alaska, winter dark periods, 1986–1997. *J. Geophys. Res.* **105,** 17267-17278 (2000).

34. Cooperative Global Atmospheric Data Integration Project. *Multi-laboratory compilation of synchronized and gap-filled atmospheric carbon dioxide records for the period 1979-2012 (obspack_co2_1_GLOBALVIEW-CO_2_2013_v1.0.4_2013-12-23)*. < http://dx.doi.org/10.3334/OBSPACK/1002> (NOAA Global Monitoring Division, Boulder, CO, 2013).

35. Mitchell, T. D. & Jones, P. D. An improved method of constructing a database of monthly climate observations and associated high-resolution grids. *Int. J. Climatol.* **25,** 693–712 (2005).

36. Tucker, C. J. *et al.* An extended AVHRR 8-km NDVI dataset compatible with MODIS and SPOT vegetation NDVI data. *Int. J. Remote Sens.* **26**, 4485–4498 (2005).

Acknowledgments

This study was supported by the National Natural Science Foundation of China (41125004), National Basic Research Program of China (2013CB956303), and National Youth Top-notch Talent Support Program in China. Philippe Ciais, Ivan A Janssens and Josep Peñuelas acknowledge support from the European Research Council through Synergy grant ERC-2013-SyG-610028 “P-IMBALANCE”.

Author contributions

S.L.P. designed the research; Z.L., T. W., and P.P.T. performed measurements of CO_2 data analysis; S.S.P., T.W., and Z.L. performed ORCHIDEE modeling and transport analysis; S.L.P. drafted the paper; and all authors contributed to the interpretation of the results and to the text.

Author Information

Reprints and permission information are available at www.nature.com/reprints. The authors have no competing financial interests. Correspondence and requests for materials should be addressed to S.L.P. (slpiao@pku.edu.cn).

Figure legend

Figure 1 Frequency distributions of the partial correlation coefficient of SZC (R_{SZC}) (**a**) and SCC (R_{SCC}) (**b**) with March-June temperature during the earliest 17 years (1979-1995) and the more recent 17 years (1996-2012). Frequency distributions of R_{SZC} and R_{SCC} were calculated through randomly selecting 14 years (the number of degrees of freedom is 10) during 1979-1995 and 1996-2012. Statistically significant partial correlation coefficient are indicated as the dotted line (magenta: $P < 0.05$ and brown: $P < 0.1$). All variables are detrended for each study period before partial correlation analysis. CFTT indicates the effect of wind change on R_{SZC} and R_{SCC}; TFCT indicates the effect of global NEE change on R_{SZC} and R_{SCC}; TFCT-B indicates the effect of boreal NEE change on R_{SZC} and R_{SCC}; TFCT-T indicates the effect of change in boreal NEE only driven by temperature on R_{SZC} and R_{SCC}; TFCT-TP indicates the effect of change in boreal NEE driven by both temperature and precipitation on R_{SZC} and R_{SCC}; TFCT-NPP indicates the effect of boreal NPP change on R_{SZC} and R_{SCC}; TFCT-HR indicates the effect of boreal HR change on R_{SZC} and R_{SCC}; TFCT-D indicates the effect of change in number of chilling days during the dormancy period on R_{SZC} and R_{SCC}.

Figure 2 Spatial distribution of difference in average partial correlation coefficient of spring carbon flux (NEE, NPP and HR) and NDVI with March-June temperature between 1996-2012 and 1979-1995. The partial correlation coefficient is calculated by statistically controlling for interannual variation in precipitation and cloud cover from March to June. Here we computed the spring carbon flux as the total flux from May to June. Carbon fluxes are derived from ORCHIDEE AR5 simulations S3 where atmospheric CO_2 and all climatic factors are varied (**a**, **b**, **c**), from simulation S1 where only temperature is varied (**d**, **e**, **f**), and from the difference

between simulation S1 and S4 where only temperature out of the dormancy period is varied (**g, h, i**). For each grid, we calculate the partial correlation coefficient through randomly selecting 14 years in the period of 1979-1995 and 1996-2012, and then take the mean value for the corresponding period. Only gridded pixels with statistically significant difference at 95% ($P<0.05$) level are shown. Note that NDVI data is only available from 1982 to 2011, so we calculate the partial correlation coefficient through randomly selecting 12 years among 1982-1996 and 1997-2011. All variables are detrended for each study period before partial correlation analysis.

Figure 3 The change in the partial correlation coefficient of simulated NEE (a), NPP (b), HR (c) and observed NDVI (d) with March-June temperature between 1996-2012 and 1979-1995 within a space of difference in number of chilling days (NCD) and number in extreme hot days (NHD) over the region north of 50 °N. Here, we define the space by each 0.5 days interval of difference in NCD and NHD between the latest period (1996-2012) and the early period (1979-1995).The NCD was calculated as the sum of days when daily air temperature was below 0 ℃ from 1st November to 30th April. The NHD was calculated as the days when temperature from March to June exceeded the 90th percentile of the temperature during 1979-2012. NEE, NPP and HR used here is from ORCHIDEE S3 simulation where both atmospheric CO_2 and all climatic factors are varied.

Figure 1

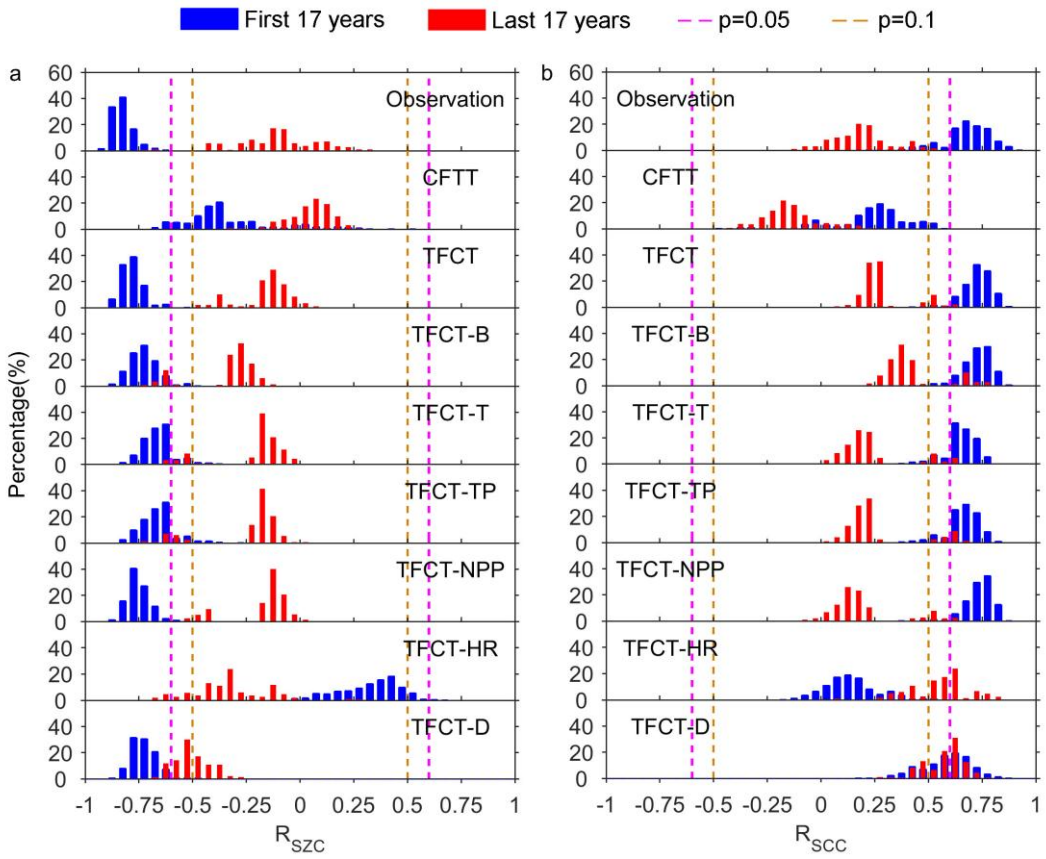

First 17 years
Last 17 years
p=0.05
p=0.1
a
b
Observation
CFTT
TFCT
TFCT-B
TFCT-T
TFCT-TP
TFCT-NPP
TFCT-HR
TFCT-D
Percentage(%)
R_{SZC}
R_{SCC}

Figure 2

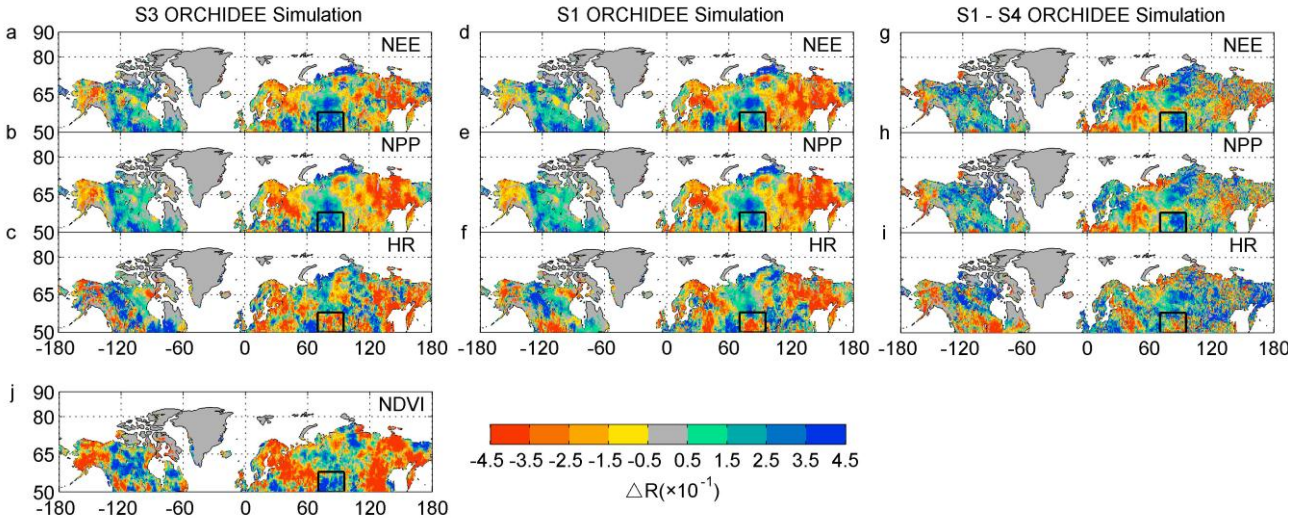
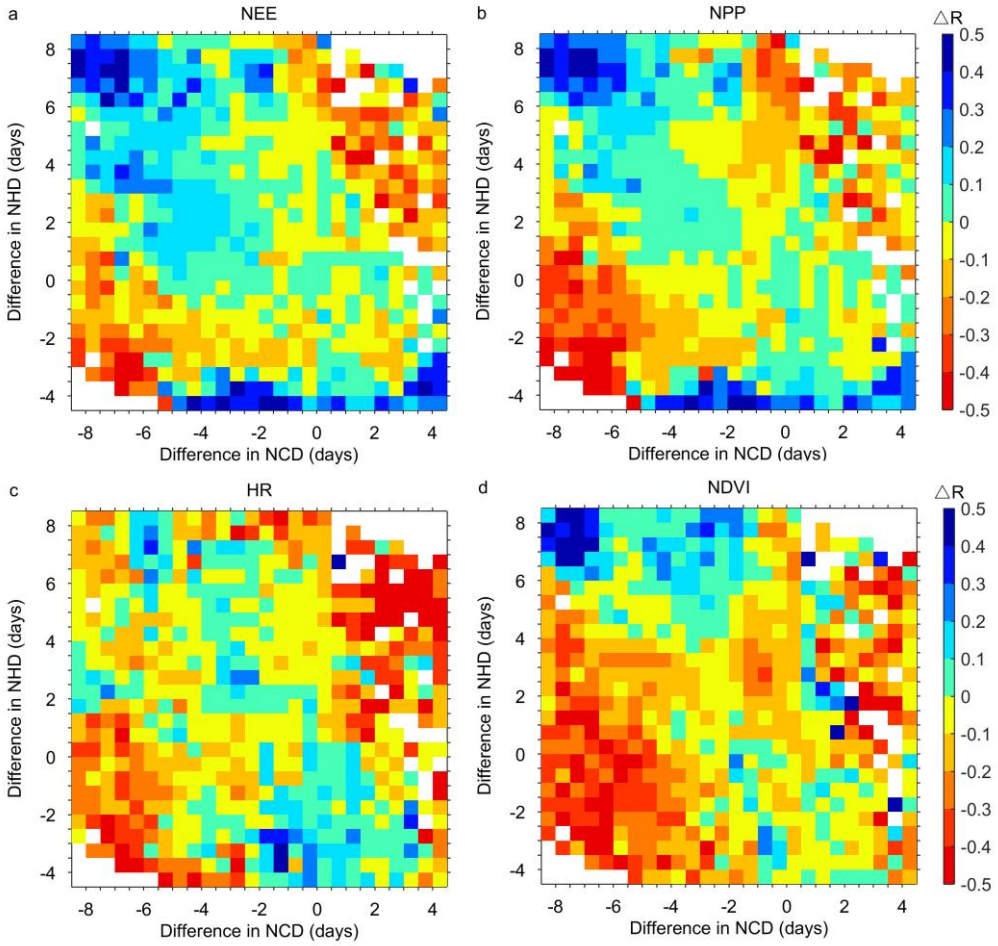

S3 ORCHIDEE Simulation
S1 ORCHIDEE Simulation
S1 - S4 ORCHIDEE Simulation
a
b
c
d
e
f
g
h
i
j
NEE
NPP
HR
NDVI
90
80
65
50
-180 -120 -60 0 60 120 180
-4.5 -3.5 -2.5 -1.5 -0.5 0.5 1.5 2.5 3.5 4.5
△R(×10-1)

Figure 3


a
NEE
b
NPP
c
HR
d
NDVI
△R
0.5
0.4
0.3
0.2
0.1
0
-0.1
-0.2
-0.3
-0.4
-0.5
Difference in NHD (days)
Difference in NCD (days)
8
6
4
2
0
-2
-4
-8
-6
-4
-2
0
2
4